33. F. Alt, N. Rosenberg, L. S. E. Thomas, D. Baltimore, *Cell* **27**, 381 (1981).
34. E. A. Kabat *et al.*, *Sequences of Proteins of Immunological Interest* (NIH, Bethesda, MD, 1987).
35. B. Seed, *Nature* **329**, 840 (1987).
36. W. J. Dower, J. F. Miller, C. W. Ragsdale, *Nucleic Acids Res.* **16**, 6127 (1988).
37. We thank R. Mosher, J. Bogan, and D. Page for the DNA's used in the Southern blot, K. Struhl for many helpful discussions, and K. Struhl, D. Black, and S. Smale for critical reading of the manuscript. Supported by NIH grant GM39458 and by fellowships from the Whitaker Health Sciences Fund (M.A.O.), and the Life and Health Insurance Medical Research Fund (O.G.S.). The GenBank accession number for the mouse RAG-2 sequence reported in this article is M33828.

30 April 1990; accepted 23 May 1990

Radar Images of Asteroid 1989 PB

STEVEN J. OSTRO, JOHN F. CHANDLER, ALICE A. HINE, KEITH D. ROSEMA, IRWIN I. SHAPIRO, DONALD K. YEOMANS

Radar observations of the near-Earth asteroid 1989 PB, made shortly after its optical discovery, yield a sequence of delay-Doppler images that reveal it to consist of two distinct lobes that appear to be in contact. It seems likely that the two lobes once were separate and that they collided to produce the current "contact-binary" configuration.

THIS ARTICLE PRESENTS RADAR OBSERVATIONS THAT PROvide two-dimensional images of a kilometer-sized asteroid and, quite unexpectedly, reveal it to have an extremely bifurcated, "double-lobed" shape. The existence of such an object has important implications for theories of the origin and evolution of asteroids and meteorite parent bodies as well as for our understanding of the cratering record of the terrestrial planets and the moon.

The imaged object, 1989 PB, is one of some 140 known near-Earth asteroids (NEAs). The NEA population is thought to include extinct cometary nuclei as well as fragments of mainbelt asteroids, and many NEAs might share (or be) the parent bodies of some meteorites (*1*). The known NEAs have sizes that range from ~50 m to ~50 km; the entire population probably contains $\sim 10^3$ objects with dimensions ≥ 1 km. Typical NEA lifetimes against collision with an inner planet or gravitational ejection from the solar system are only 10^7 to 10^8 years, but the lunar cratering record indicates that the flux of impacting projectiles has not changed very dramatically during the past 3 billion years, implying a balance between average rates of NEA depletion and replenishment (*2*). NEAs are among the most accessible objects for spacecraft rendezvous missions, but they are very difficult to study with ground-based optical telescopes and their physical characteristics are poorly known (*3*).

Radar observations can resolve NEAs spatially if the echoes are strong enough. On 9 August 1989, Helin (*4*) discovered a rapidly moving object on photographic plates taken at Palomar Observatory. Two days later, orbital calculations showed that the asteroid, designated 1989 PB by the Minor Planet Center (*5*), was approaching Earth and would pass through the Arecibo Observatory's declination window during 19–22 August at distances likely to provide echoes much stronger than in previous asteroid radar investigations (*6*). The asteroid would make its closest approach to Earth (0.027 AU, or 11 lunar distances) on 25.2 August UTC, while the Voyager 2 spacecraft was making its closest approach to Neptune. The Goldstone 70-m antenna was occupied with Voyager communications throughout the Neptune encounter and it was unavailable for use as a radar telescope until 30 August. We observed 1989 PB at Arecibo on 19–22 August and at Goldstone on 30 August (Table 1), and here we report our principal results.

Orbit refinement. Radar observations place stringent demands on the accuracy of predictions of echo time delay and Doppler frequency as well as pointing coordinates (*7*). However, errors in prediction ephemerides for freshly discovered NEAs grow rapidly, since orbits must be estimated from optical astrometric data that span short arcs. Uncertainties in a 19 August ephemeris based on optical observations obtained through 11 August (including "prediscovery" measurements found on photographic plates dating back to 1 August) would have compromised the radar observations and may even have prevented detection of echoes altogether. Optical measurements of the position of 1989 PB during 12–18 August were hampered by the nearby, nearly full moon. Fortunately, R. McNaught made critical astrometric measurements during 12–15 August at Siding Spring Observatory, Australia. In addition, two observers in Great Britain (J. D. Shanklin at Cambridge and B. Manning at Stakenbridge) made useful measurements during the 17 August total lunar eclipse.

On 19 August, using an ephemeris based on optical data from 1 to

Table 1. Geocentric distance, right ascension (RA), and declination (DEC) for radar observations of 1989 PB at epochs of the asteroid's Arecibo transit on 19–22 August and the midpoint of Goldstone observations on 30 August.

Date (1989)	Time (UTC) (hh:mm)	Distance (AU)	RA (h)	DEC (deg)	Observatory	Wavelength (cm)
19 Aug	06:33	0.060	23.93	7.0	Arecibo	13
20 Aug	06:34	0.052	0.01	11.3	Arecibo	13
21 Aug	06:36	0.044	0.13	17.2	Arecibo	13
22 Aug	06:43	0.037	0.30	25.4	Arecibo	13
30 Aug	19:35	0.057	10.78	45.0	Goldstone	3.5

S. J. Ostro, K. D. Rosema, and D. K. Yeomans are at the Jet Propulsion Laboratory, California Institute of Technology, Pasadena, CA 91109. J. F. Chandler and I. I. Shapiro are at the Harvard-Smithsonian Center for Astrophysics, 60 Garden Street, Cambridge, MA 02138. A. A. Hine is at the National Astronomy and Ionosphere Center, Box 995, Arecibo, PR 00613.

Table 2. Radar astrometric results for asteroid 1989 PB. Measurements correspond to echoes from the estimated position of the asteroid's center of mass. Epochs are referred to the instant of reception at the telescope reference point, which for Arecibo is the center of curvature of the telescope's main reflector and for Goldstone is the top of the antenna cone. Uncertainties are estimated standard errors.

Date (1989)	UTC hh:mm:ss	Observatory	Transmitter frequency (MHz)	Doppler frequency (Hz)	Time delay (UTC μs)
19 August	06:23:00	Arecibo	2380	223,401 ± 2	
	07:04:00	Arecibo	2380		59,512,323 ± 10
	07:14:00	Arecibo	2380		59,456,416 ± 10
	07:23:00	Arecibo	2380		59,406,173 ± 10
20 August	05:42:00	Arecibo	2380	215,029 ± 2	
	07:16:00	Arecibo	2380	211,450 ± 1	
21 August	06:14:00	Arecibo	2380		44,374,924 ± 3
	06:18:00	Arecibo	2380		44,354,892 ± 3
	07:24:00	Arecibo	2380	195,785 + 1	
22 August	06:45:00	Arecibo	2380	173,116 ± 1	37,453,066 ± 2
30 August	19:35:00	Goldstone	8495	−785,297 ± 8	

15 August, we detected strong echoes almost immediately. Radar measurements of echo Doppler frequency and time delay can help to ensure that newly discovered Earth-approaching asteroids will not be "lost" (*8*). Accordingly, we devoted 19 August to increasingly precise radar astrometry, ultimately reducing the asteroid's distance uncertainty on that date from the a priori value of 20,000 km to <2 km by the end of the observing session. The astrometric results from 19–22 and 30 August are presented in Table 2, and estimates of orbital elements calculated from all the currently available radar and optical data are presented in Table 3.

Asteroid 1989 PB passes very close to the orbits of Venus, Earth, and Mars twice on each revolution, since its perihelion and aphelion distances bracket all three planetary semimajor axes. The minimum orbit separations are 0.064, 0.020, and 0.061 AU, respectively. In the absence of orbit-orbit resonances or orbit evolution, the asteroid would eventually approach each planet at the minimum distance, but the many moderately close approaches to these three planets, as well as to Mercury, make it difficult to predict the long-term behavior of the orbit. The asteroid's present orbital period is fairly close to resonances with those of all three bracketed planets, so that, for example, the closest approach to Mars between 1950 and 2000 is actually 0.210 AU. Further investigation is needed to determine whether the asteroid is librating about any of the resonances; for example, the asteroid's present orbital period appears to be within one part in 10^4 of 7/12 times that of Mars.

1989 PB will pass Earth at a distance of 0.13 AU in April 1993 and at a distance of 0.12 AU in August 2012. Because of the uncertainty in long-term extrapolation of the asteroid's orbit, the geometry of close approaches to Earth more than a few decades into the future cannot be predicted with confidence. Nevertheless, it seems clear that an approach as close as the one in 1989 will not occur before 2046.

Imaging observations. During 20–22 August, our strategy focused increasingly on determination of 1989 PB's physical properties. On 20 and 21 August we emphasized "cw" runs, in which we transmitted an unmodulated continuous wave and measured the distribution of echo power as a function of frequency. The resultant echo spectra can be thought of as one-dimensional images, or scans across 1989 PB's "disc" through a slit parallel to the asteroid's apparent spin vector. The observing time on 22 August was devoted to delay-Doppler runs, in which a time-coded waveform was transmitted and the distribution of echo power in time delay and frequency was measured, yielding two-dimensional images of the asteroid. Figure 1 shows 1989 PB's rotation phases for the 20–22 August Arecibo runs discussed here.

For the cw runs, spectra were acquired in the same circular polarization as transmitted (the SC sense) and in the opposite (OC) sense (Fig. 2). The steep edges of the OC spectra are typical of echoes from small asteroids and comet nuclei (*6, 9*). The presence of appreciable backscatter all the way to the target's limbs indicates that limb-darkening can be neglected at radar wavelengths; that is, the echo power from each surface element is approximately proportional to its projected area. This result, and the ratio of the asteroid's radar cross sections for the two circular polarizations (SC/OC = 0.3 at both 13 cm and 3.5 cm), indicate that the surface is rough at centimeter-to-meter scales.

Table 3. The orbit for asteroid 1989 PB, determined from the radar data (Table 2) and 74 optical astrometric (right ascension, declination) measurements made by various observers during 1 to 25 August 1989, and reported to the Minor Planet Center (*5*). We assumed a 1 arc sec standard error in each optical measurement. The postfit, rms ratio of residual to measurement standard error for all the astrometry (that is, root reduced chi-square) is 1.1. The resulting orbital parameters, referred to the ecliptic plane and mean equinox of B1950.0, follow. Our estimate of the standard error in each of these values is about one in the last decimal place shown, based in part on a comparison of independent solutions performed at the Center for Astrophysics and the Jet Propulsion Laboratory by means of the PEP740 and DE118 planetary ephemerides, respectively.

Epoch: 1990 Nov. 5.0 TDT = JD 2448200.5	
Semimajor axis, a	1.06316 AU
Eccentricity, e	0.483223
Inclination, i	8.8883°
Longitude of ascending node, Ω	325.097°
Argument of perihelion, ω	121.192°
Mean anomaly, M	336.00°
Mean motion, n	0.89910° per day
Period	1.09626 year

A convex, nearly axisymmetric object would be expected to have OC echo spectra with peaks near the central frequency, that is, in the band that contains echoes from the subradar region and hence from the region with the largest projected area per unit frequency interval. Such a signature characterizes echoes obtained for the inner planets, natural satellites, and main-belt asteroids. However, the OC spectra obtained for 1989 PB at phases 178° and 191° show a deep central dip, suggesting that at those orientations we see a deficit, rather than an abundance, of material in the "middle" of the asteroid. (The double-peaked spectral signature vanishes abruptly, over a range of less than 6° of phase, effectively ruling out an explanation of the dip in terms of a convex shape possessing variations in surface reflectivity.) Also, the OC curve plunges in the center while the SC curve does not, so we are seeing a surge in the SC/OC ratio that depends

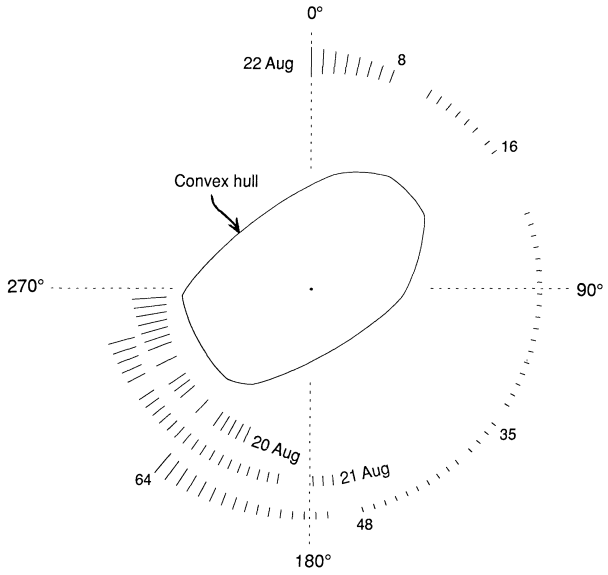

Fig. 1. Phases of cw (20 and 21 August) and delay-Doppler (22 August) Arecibo observations of 1989 PB, based on an apparent rotation period of 4.07 hours. The phase origin corresponds to 22 August 1989, $5^h27^m24^s$ UTC, which is the midpoint of echo reception for the first run on 22 August. Lengths of the radial line segments are proportional to background noise level. Variations in noise level on a given date reflect the zenith-angle dependence of the Arecibo telescope's sensitivity. The text describes estimation of the convex hull, or envelope, on the asteroid's pole-on silhouette. The hull can be thought of as the shape of a rubber band stretched around that silhouette. The central dot is the asteroid's projected center of mass. The line segment for any given run gives the radar's orientation with respect to the hull; lines for five of the 22 August runs are labeled with run numbers. For example, at 56°, in the gap between runs 16 and 17 on 22 August, the radar had an "end-on" view of the asteroid.

strongly on target orientation. This is a common signature of double-reflection backscatter from two nearly perpendicular surfaces (*10*). Therefore, the first few spectra in Fig. 2 suggest that at least at some rotation phases, we were looking into the central concavity of an object whose shape is severely bifurcated.

On 22 August, using an ephemeris that incorporated the 19–21 August radar astrometry, we did a 2.5-hour sequence of 64 delay-Doppler runs that yielded the images shown in Fig. 3. In each of the 64 images, echo time delay (distance from the radar) increases from top to bottom and Doppler frequency increases from left to right. For a rotating rigid body, the frequency of the echo from a surface element is linearly proportional to the element's distance from the plane, Ψ_0, that contains both the target's apparent spin vector and the radar. The resolution bins in Fig. 3 are, therefore, defined by constant-delay planes normal to the line of sight and constant-frequency planes parallel. (It is useful to think of each frame in Fig. 3 as the projection of the target's radar brightness onto a plane that contains the line of sight and is normal to Ψ_0.)

The 2-μs time resolution is equivalent to a distance, or range, resolution Δy = 300 m. The length equivalent of the frequency resolution, Δf = 0.95 Hz, is $\Delta x = [(\Delta f)P\lambda/4\pi]/\cos\delta$, with P the apparent rotation period and δ the angle between the asteroid's equatorial plane and the radar line of sight. The 64-frame sequence shows 1989 PB rotating counterclockwise, with an apparent spin period near 4 hours. Evidence that P = 4.07 hours is provided by (i) comparison of echoes from 20, 21, 22, and 30 August, including five delay-Doppler images from 21 August not presented here; (ii) the hull estimation described below; and (iii) photoelectric light

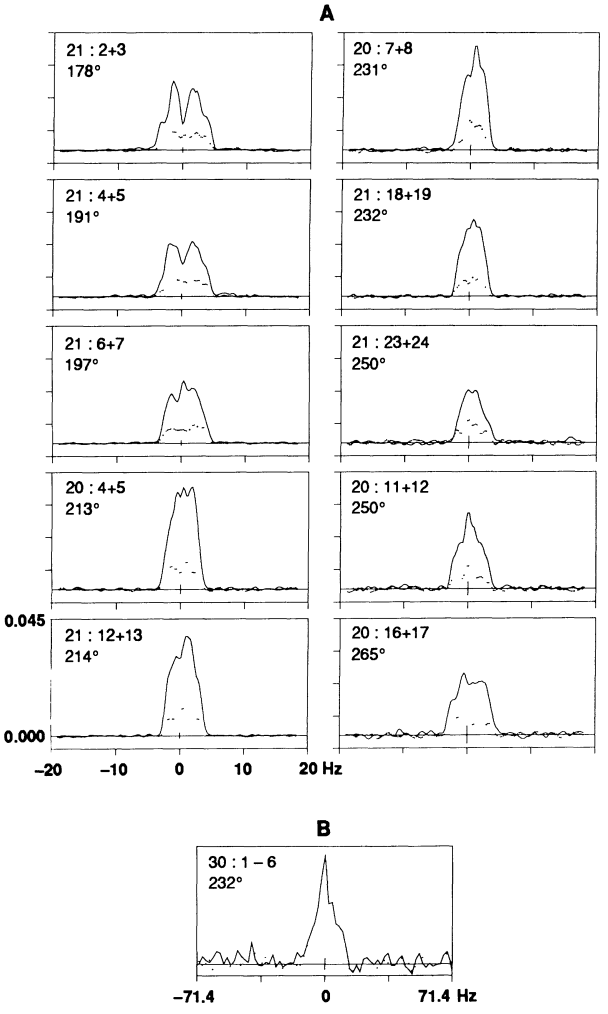

Fig. 2. (**A**) Arecibo echo spectra for asteroid 1989 PB obtained in the OC and SC polarizations (solid and dotted curves, respectively) from cw runs on 20 and 21 August. Each spectrum is a two-run weighted mean. Labels identify the August date, the two runs summed, and the runs' mean rotation phase (see Fig. 1). Echo power, in square kilometers of radar cross section per 0.95-Hz frequency bin, is plotted versus frequency. The origin at 0 Hz corresponds to hypothetical echoes from the asteroid's center of mass. The vertical bar at the origin indicates ±5 standard deviations of the receiver noise. The dominant source of statistical error at echo-containing frequencies is "self noise," whose fractional root-mean-square (rms) fluctuation is ~11% of the spectral estimates (see Fig. 3 caption). The "raw" spectra, whose resolution was 0.24 Hz, were the convolution of the "true" echo spectra with the response function of the Fourier transform used in the data reduction. That response function's ~4% side lobes and our coarsening of the spectral resolution to 0.95 Hz are responsible for the "tail" on the spectral edges. In other words, these curves understate the steepness of the edges of the asteroid's echo spectra. (**B**) Weighted mean of Goldstone spectra obtained from six cw runs within a 15-min period on 30 August (Table 1). The rotation phase of 232° is based on an apparent rotation period of 4.07 hours and the origin used in Fig. 1. Echo power is plotted on an arbitrary linear scale versus frequency. The vertical bar at the origin indicates ±1 standard deviation of the receiver noise, which overwhelms echo self-noise here. The raw frequency resolution was 2.0 Hz; these spectra have been smoothed to a resolution of 3.4 Hz. The length equivalents, in units of kilometers per cos δ, of the abscissas in (A) and (B) are identical.

curves (*11*). That value of P, which was used to assign rotation phases in Fig. 1, implies that $\Delta x = 140$ m/cos δ. Several independent lines of evidence indicate that δ was within a few tens of degrees of zero on 22 August (*12*). Therefore, we can think of the images as showing an approximately pole-on projection of 1989 PB, with the radar illumination coming from the top of the page and pixel values encoding the strength of echoes backscattered toward the top of the page. For simplicity, we constructed Fig. 3 using $\Delta x = 150$ m, which corresponds to $\delta = 21°$. Images constructed for any value of Δx between 140 and 180 m (corresponding to $|\delta| \leq 40°$) would not look very different.

Estimation of convex hull: Center-of-mass location in the images. The bandwidth of an asteroid's instantaneous echo power spectrum is proportional to the breadth, measured normal to the line of sight, of the asteroid's pole-on silhouette. Measurements of echo edge frequencies as functions of rotation phase can be used to estimate the shape (and the size in units of kilometers per cos δ) of the convex envelope, or "hull," of the pole-on silhouette as well as the offset, f_0, of the frequency of hypothetical echoes from the asteroid's center of mass (COM) from the ephemeris prediction. The hull can be thought of as the shape of a rubber band stretched around that silhouette. The COM's location in projection within the hull and the Fourier-series expansion of the hull's shape depend on f_0, which is treated as a free parameter in the least-squares estimation procedure (*13*). Uncertainties quoted for quantities related to the hull calculation are estimated standard errors.

Figure 1 shows an estimate of 1989 PB's hull derived from the 20–21 August spectra and the 22 August images; this estimation yielded values of COM frequency offsets for each date (Table 2) as well as a value of 4.07 ± 0.02 hours for the rotation period. The ratio of the pole-on silhouette's extreme breadths is 1.7 ± 0.2. The minimum bandwidth (6.2 ± 0.5 Hz) occurs within a few degrees of phase 56°, in the beginning of the longest gap in the 22 August observations (Fig. 1), just past frame 16 in Fig. 3. The maximum bandwidth (10.4 ± 0.5 Hz) occurs within a few degrees of 131°, in the middle of row 5 in Fig. 3. The corresponding extreme breadths of the silhouette are 0.91 and 1.53 km/cos δ. If our view were exactly equatorial, the asteroid's maximum range extent would be six bins, but some 50% of that extent might be hidden. We suspect that our view was not exactly equatorial, because frames near #16 show echo in five or six bins. On the other hand, if δ were, say, ~25° then we would expect to see some 80% of the full range extent of a target as elongated as 1989 PB. All factors considered, the extreme dimensions of 1989 PB's pole-on silhouette appear to be within 15% of 1.0 × 1.7 km.

The estimate of the 22 August frequency offset, $f_0 = 3.5 \pm 0.5$ Hz, establishes the absolute horizontal position of the COM in each frame. An error in the ephemeris's COM frequency prediction is

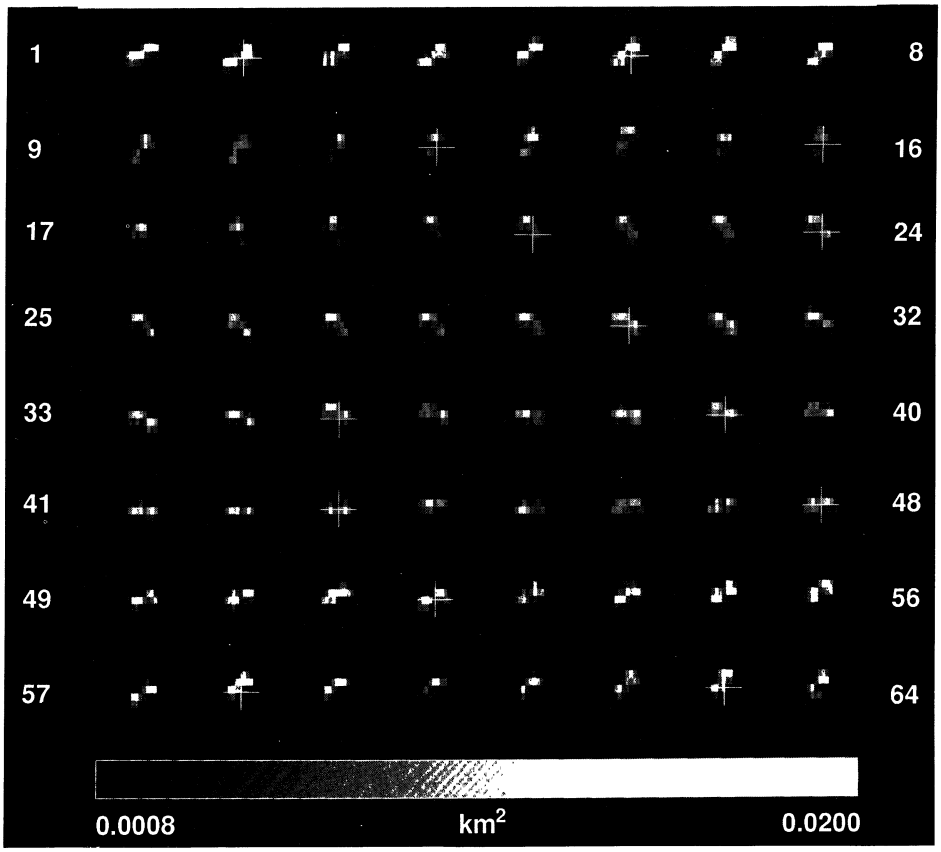

Fig. 3. Radar images of asteroid 1989 PB from Arecibo delay-Doppler runs on 22 August. The frames are numbered 1 to 8 in the top row, 9 to 16 in the second row, and so on, and have rotation phases given in Fig. 1. In each frame, echo power is plotted versus time delay (increasing from top to bottom) and frequency (increasing from left to right). The radar lies toward the top of the page, in the image plane. Resolution bins are 2 μs by 0.95 Hz, corresponding to linear dimensions of 300 m by ~150 m, as discussed in the text. In 14 frames, cross hairs indicate the estimated location of the asteroid's (projected) center of mass; the uncertainty here is probably less than one pixel. These runs used a binary-phase-coded cw waveform (*7*) with 2-μs elements and an 8191-element code that provides 8191 independent range bins, only 16 of which are shown. The relation between bin number and absolute time delay is known to within 1 μs. The effective impulse response function of the radar system (that is, of the combination of the transmitted waveform and the data acquisition/reduction) is extremely sharply peaked, with the highest side lobes no higher than several percent. Since each frame is the sum of 27 independent power spectra, or "looks," we expect errors in the resultant spectral estimates to have an rms error of 19%. The dominant source of statistical error in the brighter pixels on the asteroid is "self noise" from fluctuations in the amplitude and phase of the echoes, introduced by small variations in the asteroid's changing orientation. Radar cross section in the OC polarization is encoded with the linear gray scale shown. (No SC images were obtained.) The images have been clipped from below at 0.0008 km^2, which corresponds to one standard deviation of the background noise for frames 1 and 64, and slightly less than six standard deviations for frames 17 to 47. The absolute calibration of the telescope's sensitivity is known to about 35%; relative, frame-to-frame uncertainties are about 15%.

equivalent to an error in the predicted rate of change of echo time delay (*14*). Indeed, the asteroid drifts slowly upward through the 64 frames. The value for f_0 implies that the relative vertical position of the COM drifted toward earlier range bins by 6.6 ± 0.9 range bins between frames 1 and 64; the consequent range "smear" per frame is <7 m. Under the geometric circumstances at hand, it seems reasonable to let the hull estimate in Fig. 1 approximate the projection of the asteroid's three-dimensional envelope onto the image plane in Fig. 3 and to assume that in any given frame, the range bin containing the earliest echoes overlaps the topmost point on that envelope. These considerations constrain the absolute vertical position of the COM in each frame. Unfortunately, in frames 7, 8, 20, 25, 38, 42, and 49, a hardware malfunction shifted the range location of the echoes by an unknown number of range bins; we have registered these seven frames with adjacent frames "by hand." The white cross hairs in Fig. 3 indicate our estimates of the COM's position for 14 frames whose range registration is deemed reliable.

Since only several dozen pixels fall on the asteroid, the rectangular-pixel display in Fig. 3 makes 1989 PB look artificially "blocky." Figure 4 shows a smoothed version of the images that probably portrays some aspects of the asteroid's appearance more realistically.

Double-lobed shape. The radar images reveal 1989 PB to consist of two distinct lobes in contact (or nearly so) near the COM. The power-versus-range distribution seen for each lobe is consistent with expectations for the OC signature of a moderately rough, and hence not very limb-darkened, small body: There is a sudden onset of echo power in the range bin(s) containing the closest parts of the lobe, where there presumably is a concentration of normally oriented area and hence more projected area than in subsequent range bins, and then the echo power falls off relatively gradually with range as average angles of incidence become increasingly oblique, fading away at the lobe's limb.

The phases of the two bimodal spectra in Fig. 2 occur in row 7 of Fig. 3. Here, because of fortuitous viewing geometry, those two one-dimensional images reveal the contact region between the lobes as well as an SC/OC surge that probably is caused by double-reflection echoes from the lobes' "inside faces." The orientations of the other spectra in Fig. 2 are too close to a minimum breadth, or "end-on," phase for frequency resolution alone to reveal the asteroid's bifurcation.

Let us designate the top (closer) and bottom (farther) lobes in frame 1 as alpha and beta, respectively. Note that the relatively high brightness associated with subradar regions is not displayed by beta in frames 14 to 23, which straddle an end-on phase (Fig. 1). Here beta is being partially cut off from the radar illumination as it passes behind alpha, so the only visible portions of beta are viewed at very oblique angles of incidence and hence appear very dim. In other words, the radar sees alpha occult beta, while from our vantage point, out of the image plane, we see a partial eclipse of beta by alpha. This eclipse sequence strongly supports our inference that the radar view of 1989 PB was within a few tens of degrees of equatorial. There are no delay-Doppler images at the other end-on phase (~236°), which presumably would show beta at least partially eclipsing alpha, although that configuration appears imminent at the end of row 8.

In frame 43, the space between the two lobes is revealed as negative topographic relief. At this "broadside" phase, the registration of the range bins on the asteroid is such that the closest one containing echoes barely covers the lobes' leading edges. The next range bin covers a greater amount of each lobe as well as most of the "waist" between the lobes. In frame 16, just before the eclipse, we see the signature of negative relief on the asteroid's receding (left) limb, which faces away from the radar in frame 43. The depth of the

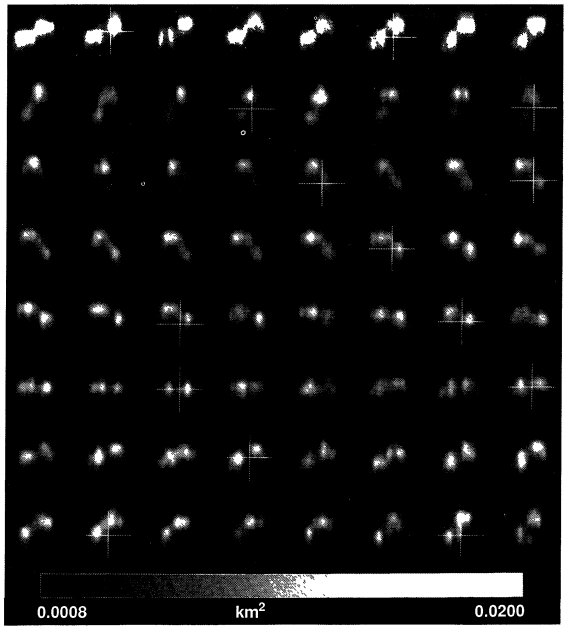

Fig. 4. A version of Fig. 3 smoothed by means of bicubic spline interpolation.

negative relief between the lobes, that is, of the two prominent concavities in the asteroid's pole-on silhouette, is probably at least a few hundred meters. The waist-to-lobe brightness ratios in Figs. 2 and 3 suggest that at rotation phases closer to broadside than to end-on, the asteroid's equatorial silhouette would show similarly prominent "polar concavities." However, there is no evidence that the two lobes are separate bodies. In particular, reductions of the radar data with frequency resolutions as fine as 0.24 Hz (spatial resolution ~40 m) do not reveal an empty gap between the two lobes, so we can state with some confidence that if the lobes are not in physical contact, they are probably no more than ~100 m apart.

Discussion. If 1989 PB consisted of two, identical, uniform-density spheres bound to each other just by their mutual gravitational attraction, then their density ρ would satisfy:

$$\rho \geq \rho_{crit} = 12\pi/GP^2 = 2.6 \text{ g cm}^{-3} \quad (1)$$

where G is the gravitation constant. The optical color indices of 1989 PB are consistent with it being an S-class asteroid (*15*). Objects in that common spectral class are thought to be mineralogically similar to stony iron or ordinary chondritic meteorites, whose typical specific gravities are 4.9 g cm^{-3} and 3.6 g cm^{-3}, respectively (*16*). Estimates of the dimensions and radar cross section of 1989 PB can be used to estimate the object's radar albedo, which can be used to constrain surface bulk density (*17*). Within the logical framework explained by Ostro *et al.* and Garvin *et al.* (*17*), our measurements indicate that the bulk density of the top few decimeters of the asteroid's surface is between 2 and 5 g cm^{-3}. Given all this information, we suggest that the spin period of 1989 PB is no greater than 1 hour more than the critical value for which the two lobes would separate, in the absence of significant tensile strength in the waist.

How did the double-lobed shape come about? It seems unlikely that the shape was "sculpted" by impacts, because this scenario would require very contrived restrictions on projectile energy and impact geometry. A more plausible hypothesis is that the asteroid's

two lobes once were separate and that a low-velocity collision between them produced the current "contact-binary" configuration. For example, Hartmann (*18*) suggested that a collision between two comparable-sized objects that shatters and disrupts them might disperse a fraction of the fragments with relative velocities low enough to produce gravitationally bound pairs, or larger groups, of fragments. Was 1989 PB born in such a "subcatastrophic" collision? If so, lobes alpha and beta may have joined soon after that event.

How common are binary and contact-binary asteroids in the near-Earth and main-belt populations? Weidenschilling *et al.* (*19*) speculated that both primordial and recent binaries might exist and noted that knowledge of the abundance of binary asteroids could constrain the collisional history of the entire main-belt population. If binary or contact-binary NEAs were plentiful, we would surmise that subcatastrophic collisions might play an important role in delivering material from the main belt into the inner solar system. An abundance of such "double" NEAs would certainly make it easier to understand the existence, on the moon and Earth, of numerous impact crater pairs that apparently were created by nearly simultaneous impact of two separated projectiles (*19*). On the other hand, if double NEAs were extremely rare, then we would favor a very different set of conclusions about the prevalence of low-velocity collisions in the main belt, the origin of doublet craters, and so forth. 1989 PB would be seen as a nearly unique relic, an isolated modern-day example of planetesimal accretion.

Radar echoes from several other asteroids show evidence for extremely irregular, nonconvex shapes (*20*), but no asteroid images as informative as those obtained for 1989 PB are yet available. Upgrades planned for the Arecibo telescope will enable images comparable to or better than those presented here to be made for an average of several NEAs per year.

REFERENCES AND NOTES

1. G. W. Wetherill and C. R. Chapman, in *Meteorites and the Early Solar System*, J. F. Kerridge and M. S. Matthews, Eds. (Univ. of Arizona Press, Tucson, 1988), pp. 35–67; E. M. Shoemaker, J. G. Williams, E. F. Helin, R. F. Wolfe, in *Asteroids*, T. Gehrels, Ed. (Univ. of Arizona Press, Tucson, 1979), pp. 253–282.
2. G. W. Wetherill, *Icarus* 76, 1 (1988); E. M. Shoemaker, *Annu. Rev. Earth Planet. Sci.* **11**, 461 (1983); P. R. Weissman, M. F. A'Hearn, L. A. McFadden, H. Rickman, in *Asteroids II*, R. P. Binzel, T. Gehrels, M. S. Matthews, Eds. (Univ. of Arizona, Tucson, 1989), pp. 880–920.
3. L. A. McFadden, D. J. Tholen, G. J. Veeder, in *Asteroids II*, R. P. Binzel, T. Gehrels, and M. S. Matthews, Eds. (Univ. of Arizona Press, Tucson, 1989), pp. 442–467.
4. E. F. Helin, *IAU Circular No. 4831* (1989).
5. B. G. Marsden, in *Asteroids*, T. Gehrels, Ed. (Univ. of Arizona Press, Tucson, 1979), pp. 77–83.
6. S. J. Ostro, in *Asteroids II*, R. P. Binzel, T. Gehrels, M. S. Matthews, Eds. (Univ. of Arizona Press, Tucson, 1989), pp. 192–212.
7. G. H. Pettengill, in *Radar Handbook*, M. I. Skolnik, Ed. (McGraw-Hill, New York, 1970), chap. 33.
8. D. K. Yeomans, S. J. Ostro, P. W. Chodas, *Astron. J.* **94**, 189 (1987).
9. J. K. Harmon, D. B. Campbell, A. A. Hine, I. I. Shapiro, B. G. Marsden, *Astrophys. J.* **338**, 1071 (1989).
10. J. Van Zyl, *IEEE Trans. Geosci. Remote Sensing* **27**, 36 (1989).
11. A. W. Harris, personal communication.
12. The lines of evidence are as follows: (i) the images show dramatic variations in the echoes' range distribution, with the extent varying from three bins near frame 43 to five or six bins near frame 15. (ii) The echo bandwidth varies from six bins near frame 15 to 11 bins near frame 43, so the ratio of extreme range extents is similar to the ratio of extreme bandwidths. (iii) The asteroid's visual light curve had an extremely high amplitude throughout late August (*11*). (iv) The echo bandwidth for a given phase during 20–22 August (as the radar line of sight changed over a 15° arc) remained virtually constant. (v) The asteroid moved some 115° on the sky between the Arecibo and Goldstone observations (Table 1), but no Arecibo/Goldstone difference in δ is discernible in the echo spectra.
13. S. J. Ostro, R. Connelly, L. Belkora, *Icarus* **73**, 15 (1988); S. J. Ostro, K. D. Rosema, R. F. Jurgens, *ibid.* **84**, 334 (1990).
14. I. I. Shapiro, M. E. Ash, M. J. Tausner, *Phys. Rev. Lett.* **17**, 933 (1966).
15. D. J. Tholen, personal communication.
16. J. A. Wood, in *The Moon, Meteorites, and Comets*, B. M. Middlehurst and G. P. Kuiper, Eds. (Univ. of Chicago Press, Chicago, 1963), pp. 573–617.
17. S. J. Ostro, D. B. Campbell, I. I. Shapiro, *Science* **229**, 442 (1985); J. B. Garvin, J. W. Head, G. H. Pettengill, S. H. Zisk, *J. Geophys. Res.* **90**, 6859 (1985).
18. W. K. Hartmann, in *Asteroids*, T. Gehrels, Ed. (Univ. of Arizona Press, Tucson, 1979), pp. 466–479.
19. S. J. Weidenschilling, P. Paolicchi, V. Zappala, in *Asteroids II*, R. P. Binzel, T. Gehrels, M. S. Matthews, Eds. (Univ. of Arizona Press, Tucson, 1989), pp. 643–658.
20. S. J. Ostro *et al.*, *Astron. J.* **99**, 2012 (1990); S. J. Ostro, D. B. Campbell, I. I. Shapiro, *Eos* 67, 1078 (1986).

21. We thank the Arecibo Observatory staff, especially A. Crespo, J. Cruz, J. Harmon, P. Perillat, A. Vazquez, R. Velez, and A. Venkataraman, for help with the Arecibo observations; R. Jurgens, D. Choate, and R. Winkler for help with the Goldstone observations; and B. Hall and R. Mortensen for image processing assistance. Part of this research was conducted at the Jet Propulsion Laboratory, California Institute of Technology, under contract with the National Aeronautics and Space Administration (NASA). The CfA experimenters were supported in part by NASA grant NAGW-967. The Arecibo Observatory is part of the National Astronomy and Ionosphere Center, which is operated by Cornell University under a cooperative agreement with the National Science Foundation and with support from NASA.

19 April 1990; accepted 11 May 1990